Neutrino-tagged jets at the Electron-Ion Collider

Miguel Arratia,[1,2] Zhong-Bo Kang,[3,4,5] Sebouh J. Paul,[1] Alexei Prokudin,[6,2] Felix Ringer,[2,7,8,9] and Fanyi Zhao[3,4,5]

[1]*Department of Physics and Astronomy, University of California, Riverside, California 92521, USA*
[2]*Thomas Jefferson National Accelerator Facility, Newport News, Virginia 23606, USA*
[3]*Department of Physics and Astronomy, University of California, Los Angeles, California 90095, USA*
[4]*Mani L. Bhaumik Institute for Theoretical Physics, University of California, Los Angeles, California 90095, USA*
[5]*Center for Frontiers in Nuclear Science, Stony Brook University, Stony Brook, New York 11794, USA*
[6]*Division of Science, Penn State University Berks, Reading, Pennsylvania 19610, USA*
[7]*Department of Physics, Old Dominion University, Norfolk, Virginia 23529, USA*
[8]*C.N. Yang Institute for Theoretical Physics, Stony Brook University, Stony Brook, New York 11794, USA*
[9]*Department of Physics and Astronomy, Stony Brook University, Stony Brook, New York 11794, USA*

(Received 23 January 2023; accepted 8 May 2023; published 30 May 2023)

We explore the potential of jet observables in charged-current deep inelastic scattering events at the future Electron-Ion Collider. Tagging jets with a recoiling neutrino, which can be identified by the event's missing transverse momentum, will allow for flavor-sensitive measurements of transverse momentum dependent parton distribution functions. We present the first predictions for transverse-spin asymmetries in azimuthal neutrino-jet correlations and hadron-in-jet measurements. We study the kinematic reach and the precision of these measurements and explore their feasibility using parametrized detector simulations. We conclude that jet production in charged-current deep inelastic scattering, while challenging in terms of luminosity requirements, will complement the Electron-Ion Collider experimental program to study the three-dimensional structure of the nucleon encoded in transverse momentum dependent parton distribution functions.

DOI: 10.1103/PhysRevD.107.094036

I. INTRODUCTION

The Electron-Ion Collider (EIC) will usher in a new era for the study of the 3D structure of the nucleon [1,2]. Its high luminosity and polarization of both electron and hadron beams will enable precise measurements of observables related to transverse momentum dependent parton distribution and fragmentation functions (TMDs).

Jets are energetic sprays of particles observed at high-energy collider experiments that are closely related to the underlying quark and gluon dynamics of hard-scattering events. Jets at the EIC will have transverse momenta up to ~ 40 GeV [3,4]. The EIC will produce the first jets in deep-inelastic scattering off transversely polarized nucleons. The potential of jets produced in neutral-current deep-inelastic scattering (NC DIS) has recently been explored, see e.g. Refs. [5–29]. In this work, we will focus on jets produced in charged-current deep-inelastic scattering (CC DIS).

The CC DIS process, which involves the exchange of a virtual $W^{\pm}$ boson, enables jet measurements that are sensitive to the flavor of the scattered quark. The leading-order process, $W^{\pm}q \to q'$, is illustrated in Fig. 1. Due to the conservation of electric charge, electrons can only scatter via the exchange of a W^- off positively charged partons, which are predominantly u quarks, especially at large x. Likewise, with a positron beam, scattering processes occur predominantly with d quarks through the exchange of a W^+ boson. Moreover, tagging either charm or strange jets can further enhance the flavor sensitivity of jet measurements [8,14,18,29–31].

The H1 and ZEUS collaborations measured inclusive CC DIS off unpolarized protons with longitudinally polarized electron and positron beams [32–37]. These measurements allowed for constraining the flavor dependence of collinear parton distribution functions (PDFs) [38]. In addition, CC DIS jet production measurements by the ZEUS collaboration [39,40], were compared to precise next-to-next-to-next-to-leading order QCD calculations [41].

One of the main challenges in measuring CC DIS is the measurement of the events' kinematic variables, Bjorken x and Q^2, in the presence of an undetected final-state neutrino. Several methods exist to address this challenge [33,42]. The feasibility studies of CC DIS at the

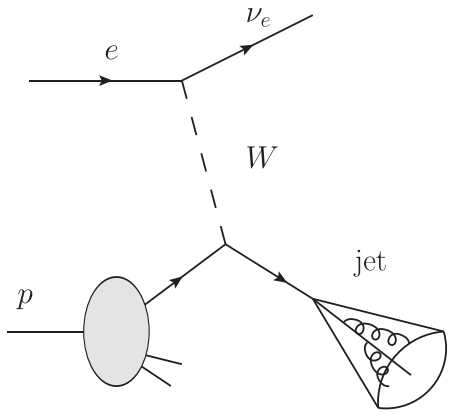

FIG. 1. Charged-current deep-inelastic scattering where the produced jet recoils against a neutrino.

EIC have been performed in Refs. [2,43] for DIS off longitudinally polarized protons with the goal to access helicity PDFs. In this study we will focus on the CC DIS off transversely polarized protons that will lead to measurements of the transverse-spin effects related to TMDs.

In semi-inclusive DIS (SIDIS), transverse-spin asymmetries can be extracted from modulations of the azimuthal angles with respect to the virtual-boson direction, typically in the Breit frame [44–48]. In CC DIS, this approach requires a measurement of the three-momentum of the scattered neutrino to define the azimuthal angle, which is challenging due to acceptance losses at forward rapidities.

Jet-based measurements of spin asymmetries can reduce these difficulties. Following Liu *et al.* [11], TMDs can be accessed in lepton-jet azimuthal correlation measurements in the laboratory frame instead of the conventional Breit frame. Liu *et al.* [11] considered NC DIS, but the formalism can be extended to CC DIS as well. The advantage of this approach is that the measurement of the azimuthal angle only requires the neutrino's transverse momentum in the lab frame, which, in general, can be measured more precisely than the full three-momentum [49]. In addition, hadron-in-jet asymmetry measurements can be performed by defining an azimuthal angle of the hadron with respect to the jet axis [15,20,50–52].

The jet-based TMD measurements have the additional advantage of decoupling initial- and final-state TMD effects (at leading power in the jet radius) [20]. That is, they do not involve a convolution of TMD PDFs and fragmentation functions which can introduce strong correlations in global fits of SIDIS data [53–57].

In this paper, we present the first study of neutrino-jet and hadron-in-jet spin asymmetries in CC DIS. We determine all possible spin asymmetries within the TMD factorization formalism. We present numerical estimates for transverse single-spin asymmetries in CC DIS. We also perform feasibility studies of these measurements using fast detector simulations and we quantify the expected kinematic reach and the statistical uncertainties.

The remainder of this paper is organized as follows. We describe the proposed measurements in Sec. II and the theoretical framework in Sec. III. We describe the fast detector simulation in Sec. IV and the expected experimental performance in Sec. V. We estimate the background in Sec. VI, and show projections for the transverse-spin asymmetries in Sec. VII. We conclude in Sec. VIII.

II. PROPOSED MEASUREMENTS

Following Liu *et al.* [11], we propose the measurement of the distribution of the azimuthal separation between the outgoing neutrino (as determined from the missing transverse momentum), and the jet. Due to the momentum conservation, the jet and neutrino are expected to be predominantly produced back to back in the transverse plane. Therefore, the azimuthal distribution is expected to be centered around $\phi_{\rm jet} - \phi_\nu - \pi = 0$, with some finite width due to out-of-cone QCD radiation and the nonzero initial momentum of the scattered quark. In the next section, we determine all spin asymmetries that can be measured in neutrino-jet and hadron-in-jet production within TMD factorization.

We note that the measurement of x requires information about the longitudinal momentum or the rapidity of the neutrino. An analogous measurement of TMDs in the Breit frame would require a measurement of the boost vector that depends on the neutrino rapidity, which would make variables such as the azimuthal angle dependent on it. See for example Ref. [10], where a (neutral-current) TMD-jet observable was proposed in the Breit frame. Therefore, we expect that the laboratory observables proposed here are better suited to perform CC TMD-jet measurements.

Moreover, we propose to measure the transverse single-spin asymmetry in neutrino-jet correlations, also known as the left-right asymmetry

$$A_{\rm UT} = \frac{{\rm d}\sigma^{\uparrow} - {\rm d}\sigma^{\downarrow}}{{\rm d}\sigma^{\uparrow} + {\rm d}\sigma^{\downarrow}}, \tag{1}$$

where, ${\rm d}\sigma^{\uparrow,\downarrow}$ refers to the differential cross section measured with transverse polarization of the initial proton pointing up or down. This asymmetry is expected to exhibit a modulation with respect to the angular separation between the incoming proton spin, ϕ_S, and the momentum imbalance, ϕ_q, i.e.,

$$A_{\rm UT} = A_{\rm UT}^{\sin(\phi_S - \phi_q)} \sin(\phi_S - \phi_q). \tag{2}$$

Here, the momentum imbalance between the jet and the neutrino is defined by $\vec{q}_T = \vec{p}_T^{\,\rm jet} + \vec{p}_T^{\,\nu}$. This asymmetry is sensitive to the Sivers function [11,16], which describes the anisotropy of unpolarized partons in a transversely polarized proton.

We also propose to perform a hadron-in-jet measurement in CC DIS of the asymmetry $A_{\rm UT}^{\sin(\phi_S - \phi_{\rm h})}$ defined for the

azimuthal angle of the hadron in jet ϕ_h. In NC DIS, the hadron-in-jet asymmetry is sensitive to both the Collins and the transversity functions [15].

There are a number of recent extractions of Sivers functions [56,58–66], transversity [56,67–73], and Collins fragmentation functions [56,67,68,72,73] from experimental data. Flavor dependence of these functions is known relatively well for the u and d quarks and poorly known for the other flavors. Charged-current measurements have the potential to provide complementary information for flavor separation.

III. THEORETICAL FRAMEWORK

In this section, we discuss inclusive jet production in CC DIS, neutrino-jet correlations, and hadron-in-jet observables.

A. Inclusive jet production

We follow the theoretical framework developed in Refs. [11,15,16,20] for the NC DIS. At the parton level, we consider the leading-order process $eq \to \nu q'$ mediated via the exchange of a virtual W boson. We consider the cross section differential in Bjorken x and the transverse momentum of the produced neutrino, p_T^ν, which is defined relative to the beam direction in the laboratory frame. The leading-order cross section can be written as

$$\frac{\mathrm{d}\sigma^{ep\to\nu\mathrm{jet}X}}{\mathrm{d}x\mathrm{d}^2\vec{p}_T^{\,\nu}} = \sum_q \sigma_0^{eq\to\nu q'} f_q(x,\mu), \tag{3}$$

where the renormalization scale μ of the PDF f_q is chosen at the order of the hard scale of the process $\mu \sim p_T^\nu$. The prefactor σ_0 for initial quarks u and $\bar{d}$ are given by

$$\begin{aligned}\sigma_0^{eu\to\nu d} &= \frac{|\overline{\mathcal{M}}_{eu\to\nu d}|^2}{16\pi^2\hat{s}^2}\frac{\hat{t}}{x(\hat{t}-\hat{u})},\\ &= 8(G_F m_W^2)^2|V_{ud}|^2\frac{\hat{s}^2}{(\hat{t}-m_W^2)^2+m_W^2\Gamma_W^2}\frac{\hat{t}}{x(\hat{t}-\hat{u})},\end{aligned} \tag{4}$$

$$\begin{aligned}\sigma_0^{e\bar{d}\to\nu\bar{u}} &= \frac{|\overline{\mathcal{M}}_{e\bar{d}\to\nu\bar{u}}|^2}{16\pi^2\hat{s}^2}\frac{\hat{t}}{x(\hat{t}-\hat{u})},\\ &= 8(G_F m_W^2)^2|V_{ud}|^2\frac{\hat{u}^2}{(\hat{t}-m_W^2)^2+m_W^2\Gamma_W^2}\frac{\hat{t}}{x(\hat{t}-\hat{u})},\end{aligned} \tag{5}$$

where G_F is the Fermi constant, m_W and Γ_W are the W boson mass and decay width, and V_{ud} is the standard Cabibbo–Kobayashi–Maskawa (CKM) matrix element. Here $\hat{t}/(x(\hat{t}-\hat{u}))$ is the Jacobian factor, which is obtained by transforming the cross section to be differential in Bjorken-x instead of the neutrino rapidity y_ν. These two variables are related by

$$x = \frac{p_T^\nu e^{y_\nu}}{\sqrt{s} - p_T^\nu e^{-y_\nu}}. \tag{6}$$

The Mandelstam variables in Eqs. (4) and (5) can be written in terms of the kinematic variables of the produced neutrino and the center-of-mass energy, namely

$$\hat{s} = xs, \tag{7}$$

$$\hat{t} = -Q^2 = -\sqrt{s}p_T^\nu e^{y_\nu} = -x\sqrt{s}p_T^{\mathrm{jet}}e^{-y_{\mathrm{jet}}}, \tag{8}$$

$$\hat{u} = -x\sqrt{s}p_T^\nu e^{-y_\nu} = -\sqrt{s}p_T^{\mathrm{jet}}e^{y_{\mathrm{jet}}}. \tag{9}$$

Here p_T^{jet} and y_{jet} denote the jet transverse momentum and rapidity, respectively.

B. Neutrino-jet correlations

Next, we discuss neutrino-jet correlations via the exchange of a W^- boson in polarized electron-proton scattering

$$p(P_A,\lambda_p,\vec{S}_T) + e(P_B,\lambda_e) \to \mathrm{jet}(P_J) + \nu(P_D) + X. \tag{10}$$

Here λ indicates the longitudinal polarization and $\vec{S}_T$ denotes the transverse spin vector of the proton. In order to access TMDs, we study back-to-back neutrino-jet production in the ep collision frame. By defining light-cone vectors $n_+^\mu = \frac{1}{\sqrt{2}}(1,0,0,1)$ and $n_-^\mu = \frac{1}{\sqrt{2}}(1,0,0,-1)$, we write the momentum of the incoming proton P_A and the electron P_B as

$$P_A^\mu = P^+ n_+^\mu + \frac{M^2}{2P^+}n_-^\mu \approx P^+ n_+^\mu = \sqrt{\frac{s}{2}}n_+^\mu, \tag{11}$$

$$P_B^\mu = \sqrt{\frac{s}{2}}n_-^\mu. \tag{12}$$

Here $s = (P_A + P_B)^2$ is the center-of-mass energy. We set the final observed jet to be produced in the xz plane, with the following momentum $P_J^\mu = E_J(1,\sin\theta_J,0,\cos\theta_J)$. Here E_J is the jet energy and the angle θ_J is measured with respect to the beam direction. We find that the differential cross section can be written in terms of the structure functions as follows[1]

[1]Notice that unlike the usual practice for SIDIS or Drell-Yan (DY) cross sections, we do not factor out the elementary cross sections from the structure functions. Our structure functions therefore become dimension-full quantities, see for instance Ref. [74].

$$\frac{d\sigma^{ep\to\nu\text{jet}X}}{dx d^2\vec{p}_T^{\,\nu} d^2 q_T} = F_{UU} + \lambda_p F_{UL} + |S_T|\Big[\sin(\phi_q-\phi_{S_A})F_{UT}^{\sin(\phi_q-\phi_{S_A})} + \cos(\phi_q-\phi_{S_A})F_{UT}^{\cos(\phi_q-\phi_{S_A})}\Big] + \lambda_e\Big[F_{LU} + \lambda_p F_{LL} + |S_T|\sin(\phi_q-\phi_{S_A})F_{LT}^{\sin(\phi_q-\phi_{S_A})} + |S_T|\cos(\phi_q-\phi_{S_A})F_{LT}^{\cos(\phi_q-\phi_{S_A})}\Big]. \quad (13)$$

The subscripts E and P of a structure function F_{EP} indicate the polarization of the incoming electron and incoming proton, respectively: U for unpolarized, L for longitudinally polarized or T for transversely polarized. For example, for unpolarized scattering, the structure function is denoted by F_{UU}. In the limit of small values of the transverse-momentum imbalance $|\vec{q}_T| \ll p_T^{\text{jet}} \sim p_T^{\nu}$, one can write this structure function in the following form using the TMD factorization formalism

$$F_{UU} = \sum_q \frac{|\overline{\mathcal{M}}_{eq\to\nu q'}|^2}{16\pi^2\hat{s}^2} H(Q,\mu)\mathcal{J}_q(p_T^{\text{jet}}R,\mu) \times \int \frac{db_T b_T}{2\pi} J_0(q_T b_T) f_1^{\text{TMD}}(x,b_T,\mu,\zeta) \times S_q(b_T,y_{\text{jet}},R,\mu). \quad (14)$$

Here $H(Q,\mu)$ is the hard function, which accounts for virtual corrections at the hard scale Q. The jet function $\mathcal{J}_q$ is associated with collinear dynamics of the jet with characteristic scale $\mu_J \sim p_T^{\text{jet}}R$ [75]. For our numerical results presented below we use the anti-k_T algorithm [76]. The quark TMD PDF including the appropriate soft factor for a generic TMD in b_T space is defined by [20,77]

$$f_q^{(n),\text{TMD}}(x,b_T,\mu,\zeta) = \frac{2\pi n!}{(M^2)^n}\int dk_T\, k_T\left(\frac{k_T}{b_T}\right)^n J_n(k_T b) \times \tilde{f}_q^{\text{TMD}}(x,k_T^2,\mu,\zeta), \quad (15)$$

where M is the mass of the nucleon and J_n is the nth order Bessel function. Here μ is the renormalization scale, while ζ is the so-called Collins-Soper scale [78]. Notice that for the unpolarized TMD f_1^{TMD}, $n=0$. The unpolarized TMDPDF $\tilde{f}_1^{\text{TMD}}(x,b_T,\mu,\zeta)$ in Eq. (13) is factorized as

$$\tilde{f}_1^{\text{TMD}}(x,b_T,\mu,\zeta) = \int_x^1 \frac{d\hat{x}}{\hat{x}} C_{q\leftarrow i}\left(\frac{x}{\hat{x}},\mu_{b_*}\right) f_1^i(\hat{x},\mu_{b_*}) \times \exp[-S_{\text{pert}}(\mu,\mu_{b_*}) - S_{\text{NP}}^f(x,b_T,Q_0,\zeta)], \quad (16)$$

where the b_* prescription is given by Ref. [79] with $b_* = b_T/\sqrt{1+b_T^2/b_{\text{max}}^2}$ and $b_{\text{max}} = 1.5\ \text{GeV}^{-1}$. In this work, we follow the TMD factorization for Sivers function shown in Ref. [63], where TMD evolution up to next-to-next-to-leading logarithmic accuracy has been provided in the Sivers extraction. The coefficient functions $C_{q\leftarrow i}$ can be found in Refs. [68,78,80–83] and the nonperturbative Sudakov factor $S_{\text{NP}}^f(x,b_T,Q_0,\zeta)$ has been parametrized in Refs. [53,63]. The remaining soft function S_q in Eq. (14) includes a contribution from the global soft function which depends on the Wilson lines in the beam and jet directions, and the collinear-soft function associated with the soft jet dynamics. Since S_q accounts for different soft contributions, it depends on both the jet rapidity y_{jet} and the jet radius R and the expression of S_q is given in [15].

The other cross sections or structure functions in Eq. (13) depend on the polarization state of the nucleon (longitudinal or transverse) and the longitudinal lepton polarization. As an example, we consider the case where the initial proton is transversely polarized. The cross section or structure function $F_{UT}^{\sin(\phi_q-\phi_{S_A})}$ sensitive to correlations of an unpolarized quark in the transversely polarized proton is given by

$$F_{UT}^{\sin(\phi_q-\phi_{S_A})} = \sum_q \frac{|\overline{\mathcal{M}}_{eq\to\nu q'}|^2}{16\pi^2\hat{s}^2} H(Q,\mu)\mathcal{J}_q(p_T^{\text{jet}}R,\mu) \times \int \frac{db_T b_T^2}{4\pi M} J_1(q_T b_T) f_{1T}^{\perp(1),\text{TMD}}(x,b_T,\mu,\zeta) \times S_q(b_T,y_{\text{jet}},R,\mu). \quad (17)$$

In this case, the structure function is related to the Bessel function of the first order $J_1(q_T b_T)$ and the Sivers function $f_{1T}^{\perp(1),\text{TMD}}(x,b_T,\mu,\zeta)$ in b_T space as defined in Eq. (15).

We provide more details about the other structure functions in Eq. (13) in Appendix A. For example, for an incoming electron with helicity λ_e, one replaces $\sigma_0^{eq\to\nu q'}$ with $\sigma_0^{e_L q\to\nu q'}$ as given in Eq. (A6).

C. Hadron distributions inside jets

In this subsection, we study the longitudinal- and transverse-momentum distributions of hadrons in the identified jet for electron-proton scattering via the exchange of a W^- boson:

$$p(P_A,\lambda_p,\vec{S}_T) + e(P_B,\lambda_e) \to (\text{jet}(P_J)h(z_h,\vec{j}_T)) + \nu(P_D) + X. \quad (18)$$

The production of unpolarized final-state hadrons at leading twist is encoded in two TMD jet fragmentation functions, $\mathcal{D}_1$ and $\mathcal{H}_1^{\perp}$ [20]:

$$\Delta(z_h,\vec{j}_T)=\mathcal{D}_1^{h/q}(z_h,j_T)\frac{\not{n}_-}{2}-i\mathcal{H}_1^{\perp,h/q}(z_h,j_T)\frac{\not{j}T}{z_hM_h}\frac{\not{n}_-}{2}. \tag{19}$$

Thus, we find the following differential cross section expressed in terms of structure functions

$$\begin{aligned}\frac{\mathrm{d}\sigma^{ep\to\nu+\mathrm{jet}X}}{\mathrm{d}x\mathrm{d}^2\vec{p}_T^{\,\nu}\mathrm{d}^2q_T\mathrm{d}z_h\mathrm{d}^2j_T}&=F_{UU}^h+\lambda_pF_{UL}^h+|S_T|\Big[\cos(\phi_q-\phi_{S_A})F_{UT}^{h,\cos(\phi_q-\phi_{S_A})}\\&+\sin(\phi_q-\phi_{S_A})F_{UT}^{h,\sin(\phi_q-\phi_{S_A})}\Big]+\lambda_e\Big[F_{LU}^h+\lambda_pF_{LL}^h\\&+|S_T|\sin(\phi_q-\phi_{S_A})F_{LT}^{h,\sin(\phi_q-\phi_{S_A})}\\&+|S_T|\cos(\phi_q-\phi_{S_A})F_{LT}^{\cos(\phi_q-\phi_{S_A})}\Big].\end{aligned} \tag{20}$$

In total, we find eight structure functions and the full expression is provided in Appendix B. Following the same convention we used in Eq. (13), the subscripts E and P of a structure function F_{EP}^h here also indicate the polarization of the incoming electron and the incoming proton, respectively. Notably, we found that none of the Collins-type jet fragmentation functions contribute in Eq. (20). The reason is that chiral-odd functions have to be coupled with another chiral-odd function, the chirality between two factors of $(1-\gamma_5)$ resulting from the weak charged-current vertices must be odd. As a result, see Eq. (B5), we always have $(1-\gamma_5)(1+\gamma_5)=0$, which implies that all terms involving chiral-odd functions vanish. This conclusion is robust at leading power of the TMD factorization formalism we are using. However, whether this still holds going beyond the leading power TMD factorization, see e.g. within TMD factorization at subleading power [84–86] or including higher loops as discussed in Refs. [87,88], needs further investigation. We leave such a study to a future publication.

Using TMD factorization at leading power, see Refs. [50–52,75,89–94], we can write the unpolarized structure function where a hadron is measured inside the jet as follows:

$$\begin{aligned}F_{UU}^h=H(Q,\mu)\sum_q\sigma_0^{eq\to\nu q'}\mathcal{D}_1^{h/q}(z_h,j_T,p_T^{\mathrm{jet}}R,\mu)\\\times\int\frac{\mathrm{d}^2\vec{b}_T}{(2\pi)^2}e^{i\vec{q}_T\cdot\vec{b}_T}f_1^{\mathrm{TMD}}(x,b_T,\mu,\zeta)S_q(b_T,y_{\mathrm{jet}},R,\mu).\end{aligned} \tag{21}$$

Here the variables $z_h=\vec{p}_h\cdot\vec{p}_{\mathrm{jet}}/|\vec{p}_{\mathrm{jet}}|^2$ and $j_T=|\vec{p}_h\times\vec{p}_{\mathrm{jet}}|/|\vec{p}_{\mathrm{jet}}|^2$ denote the longitudinal momentum fraction and the transverse momentum relative to the (standard) jet axis of the hadron inside the jet, respectively. In the factorized cross section in Eq. (21), $\mathcal{D}_1^{h/q}$ is a TMD fragmenting jet function. It describes the hadron-in-jet measurement and replaces the jet function $\mathcal{J}_q$ in Eq. (14). At next-to-leading logarithmic (NLL) accuracy, we can write $\mathcal{D}_1^{h/q}$ as

$$\begin{aligned}\mathcal{D}_1^{h/q}(z_h,j_T,p_T^{\mathrm{jet}}R,\mu)\\=\int\frac{\mathrm{d}^2\vec{b}_T'}{(2\pi)^2}e^{i\vec{j}_T\cdot\vec{b}_T'/z_h}D_1^{q/h}(z_h,\vec{b}_T',p_T^{\mathrm{jet}}R).\end{aligned} \tag{22}$$

Here we work in Fourier conjugate space and $D_1^{q/h}$ is a TMD fragmentation function (TMDFF) evaluated at the jet scale. We use the Fourier variable $\vec{b}_T'$ here to indicate that there is no convolution of the TMD fragmentation function with the TMD PDF in Eq. (21). Also note that the TMDFFs can be matched to the collinear FFs [78,80] and in this work, we apply the extraction of collinear fragmentation functions in [95] for constructing the TMDFFs. See Ref. [93] for more details.

IV. SIMULATION

In this section, we discuss Monte Carlo event-generator results for neutrino-jet correlations as well as detector-response simulations. We show comparisons between theoretical calculations discussed in the previous section and the Monte Carlo simulations for unpolarized cross sections in CC DIS events.

A. Event generation with PYTHIA8

We used PYTHIA8 [96] to simulate CC DIS events in unpolarized electron-proton and positron-proton collisions. We choose the energies of the incoming electron and proton as 10 GeV and 275 GeV, respectively. These beam-energy values, which yield a center-of-mass energy of $\sqrt{s}=105\,\mathrm{GeV}$, correspond to the operation point that maximizes the luminosity of the EIC design [97]. Following Ref. [43], we selected events with $Q^2>100\ \mathrm{GeV}^2$. QED radiative effects [98,99] are not included in the simulation to match the calculations in Sec. III.[2] We used the FASTJET3.3 package [101] to reconstruct jets with the anti-k_T algorithm [76] and jet radius parameter $R=1$. The input particles for the generator-level jet-finding algorithm are all stable particles ($c\tau>10$ mm), except for neutrinos.

Figure 2 shows our theoretical results at NLL accuracy for the transverse momentum imbalance of the neutrino and jet q_T/p_T^{ν}. In addition, we show the PYTHIA8 simulations for unpolarized CC DIS events. The theoretical uncertainties are obtained by varying the scales renormalization scale $\mu\sim p_T^{\mathrm{jet}}$ and the jet scale $\mu_J\sim p_T^{\mathrm{jet}}R$ by a factor of 2 around their central values and taking the envelope. We observe

[2]Based on similar measurements in NC DIS [100], the QED corrections are expected to be small for the observables considered in this work. Therefore, we do not expect that our conclusions are affected by these effects.

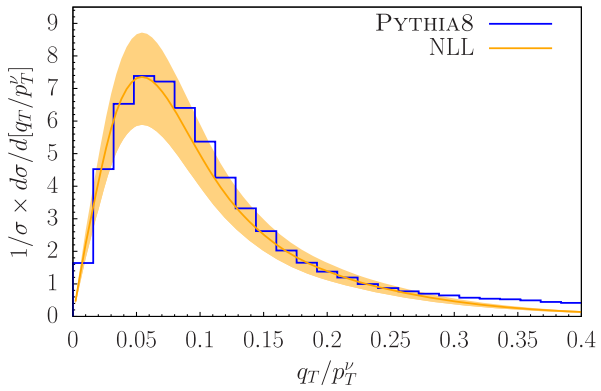

FIG. 2. Normalized distribution of the neutrino-jet imbalance momentum q_T/p_T^ν in unpolarized electron-proton scattering via the exchange of a W^- boson. We show our theoretical results at NLL accuracy with QCD scale uncertainties (orange) compared to Monte Carlo event-generator simulations obtained with PYTHIA8 [96] (blue).

good agreement between the resummed TMD calculation at NLL and the PYTHIA8 results. However, the tail of the q_T/p_T^ν distribution falls slower at high q_T/p_T^ν for the PYTHIA8 simulations compared to the resummed TMD result. This is likely due to multijet events, which are not included as a matching contribution in the TMD result at large q_T.

Figure 3 shows our theoretical results including QCD scale uncertainties (we again take the envelope of the results when varying the scales $\mu \sim p_T^{\text{jet}}$ and $\mu_J \sim p_T^{\text{jet}} R$ by a factor of 2 around their central values) for the longitudinal z_h and transverse momentum j_T distributions for $\pi^\pm$ compared to the PYTHIA8 results. We use the same simulated event sample as described above, and we observe reasonable agreement between the two results.

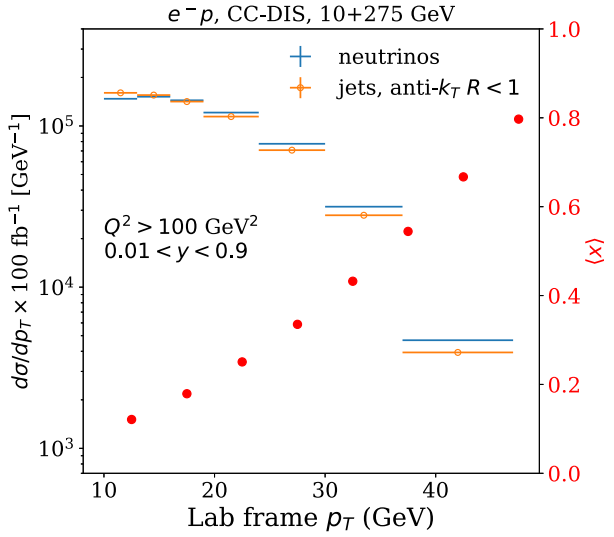

FIG. 4. Expected yield of neutrinos and jets in CC DIS events with an electron beam and 100 fb^{-1} integrated luminosity. In addition, we show the average parton momentum fraction x, which is probed as a function of the neutrino transverse momentum in the laboratory frame. The cross sections generated in PYTHIA8 have been scaled to match the total cross section calculated at next-to-leading order in Ref. [43].

Lastly, Fig. 4 shows the neutrino yields expected for 100 fb^{-1}, which can be collected in about a year of running at 10^{34} cm^{-2} s^{-1}, as a function of the neutrino's transverse momentum. We also show the mean of the parton momentum fraction x as a function of transverse momentum (red dots). Values up to $x = 0.8$ can be probed with jet/neutrino transverse momenta of $p_T = 45$ GeV, which corresponds to the kinematic limit. With 100 fb^{-1}, the statistical uncertainty of the cross section measurement

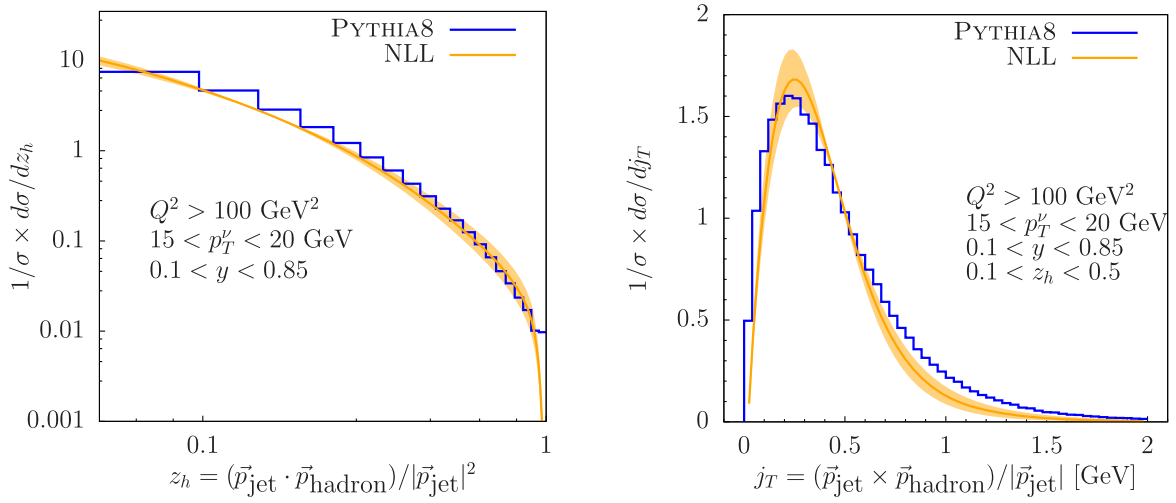

FIG. 3. Distributions of the $\pi^\pm$-in-jet longitudinal-momentum fraction z_h (left) and the transverse momentum j_T (right) in CC DIS events. We show our theoretical results at NLL accuracy with QCD scale uncertainties (orange) compared to Monte Carlo event-generator simulations obtained with PYTHIA8 [96] (blue).

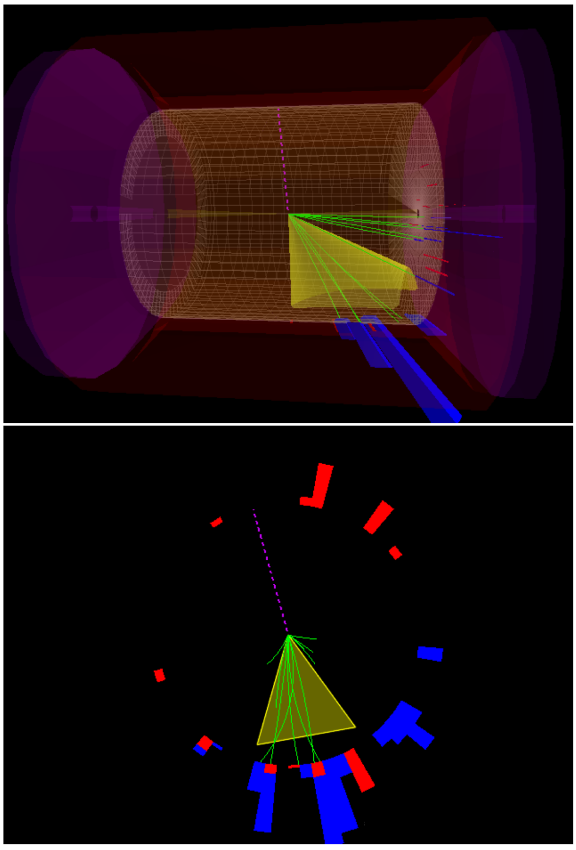

FIG. 5. Display of a simulated CC DIS event using DELPHES [102]. Top: 3D view. Bottom: transverse view.

is expected to be negligible over the entire kinematic range. However, high luminosity is needed to measure the corresponding spin asymmetries, as will be further discussed in Sec. VII below.

B. Detector-response simulations

We use the DELPHES package [102] to perform fast detector simulations with parameters specified in Ref. [103]. We consider a general-purpose detector geometry including tracking, electromagnetic and hadronic calorimeters with coverage up to $|\eta| = 4.0$ and full azimuthal coverage, as described in the EIC Yellow Report [2]. This is in line with proposed EIC detector design [104–106] that considered a high degree of Hermeticity, which can be ensured with dedicated detectors at forward angles [107]. We show a representative charged-current event in Fig. 5.

To reconstruct jets in the detector-response simulation, we use again the FASTJET3.3 package [101] with the anti-k_T algorithm [76] and $R = 1$ [108]. As input to the jet algorithm, we use the set of particle-flow objects reconstructed with DELPHES.

In Fig. 6, we show the hadron-in-jet momenta for reconstructed $\pi^{\pm}$, as well as the average z_h in each momentum bin. We find that the charged pions in jets are mostly in $-0.5 < \eta < 3.5$, and have momenta up to

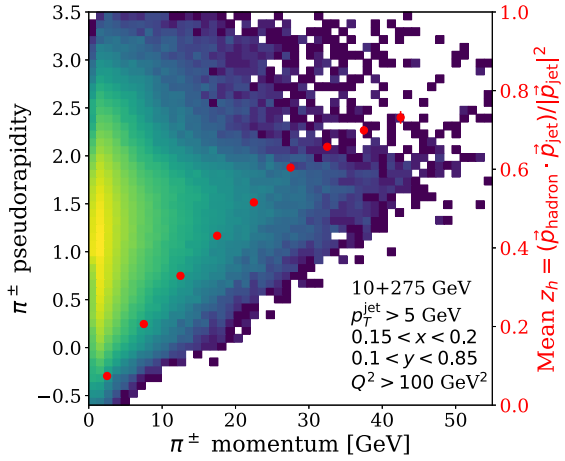

FIG. 6. Pseudorapidity and momentum distribution of charged pions in jets with $p_T > 5$ GeV in ep CC DIS. The average longitudinal-momentum fraction of the hadron with respect to the jet axis is shown by the red dots.

about 45 GeV, which can be identified with high purity using gas-based Cherenkov detectors [2].

V. EVENT RECONSTRUCTION AND KINEMATIC RESOLUTION

As typically done at particle colliders, neutrinos can be identified by measuring the missing transverse momentum, $\vec{p}_T^{\,\text{miss}}$, which is defined as the vector sum of the transverse momenta of all measured particles (identified using the particle-flow algorithm to avoid double counting).

In this section we estimate the performance of this reconstruction method for EIC. We expect this estimate to be reasonable given that the DELPHES fast smearing was shown to reproduce reasonably well the performance obtained from a comprehensive detector simulation of the Compact Muon Solenoid (CMS) experiment down to about $|p_T^{\text{miss}}| = 20$ GeV [102].

We define ϕ_ν as the azimuthal angle of $-\vec{p}_T^{\,\text{miss}}$. We show the reconstruction performance of ϕ_ν in Fig. 7. The standard deviation is less than 0.06 radians, which is of similar order as the dijet azimuthal-angle resolution of the measurement presented in Ref. [109].

We employ the Jacquet-Blondel (JB) method of Ref. [110] to reconstruct the lepton kinematics. The event inelasticity is given by $y_{\text{JB}} = \sum(E_i - p_{z,i})/(2E_e)$, where the sum is over all the reconstructed particles. The four-momentum transfer is given by $Q^2_{\text{JB}} = (p_T^{\text{miss}})^2/(1 - y_{\text{JB}})$ and the Bjorken scaling variable is $x_{\text{JB}} = Q^2_{\text{JB}}/(s y_{\text{JB}})$, where $s = 4E_eE_p$ and E_e (E_p) is the energy of the electron (proton) beam. The resolution of reconstructing these variables for inclusive DIS was investigated in Refs. [14,43], and was found to be reasonable for all three of these variables. The performance of the Jacquet-Blondel method might be improved with machine-learning methods such as those proposed in Refs. [111–114].

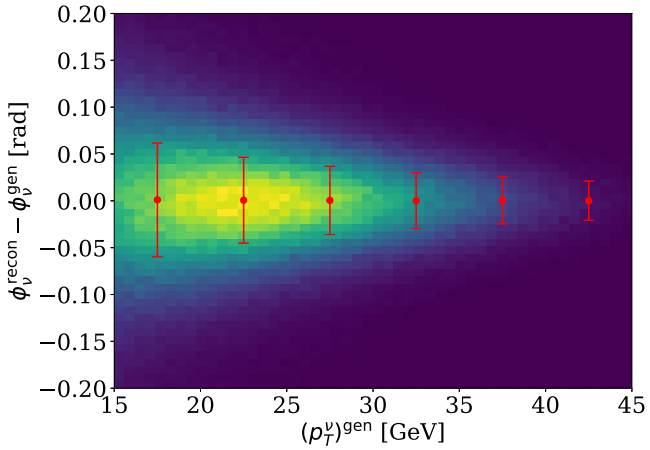

FIG. 7. Performance of the reconstruction of ϕ_ν in CC DIS events. The red error bars indicate the means and standard deviations for given slices of p_T^ν.

In Fig. 8, we compare the reconstructed values of q_T/p_T^ν with the values obtained at generator level. We chose the number of bins such that the expected bin purity, the fraction of generated events that are reconstructed in the same bin, is at least 50%. At this level, the proposed binning is amenable to standard unfolding methods. The bin purity is shown in the bottom panel.

VI. SUPPRESSION OF THE BACKGROUND FROM NC DIS AND PHOTOPRODUCTION

Given the relatively low rate of charged-current DIS events relative to neutral-current DIS and photoproduction, the background suppression generally represents a significant challenge. If the scattered electron is missed, the event topologies of neutral- and charged-current DIS can become identical. We expect that this scenario will be significantly suppressed at the EIC compared to the HERA experiments due to improved low-angle taggers for low-Q^2 events [2], although the performance of these systems is hard to estimate at this point.

Rather than using a low-angle scattering veto to suppress photoproduction, we follow the approach used by the CC DIS analyses at HERA [33] which relied on two kinematic variables: $\delta = \sum_i E_i - p_{z,i}$ (where E_i and $p_{z,i}$ are the reconstructed energy and longitudinal momentum of detected particles, and the sum runs over all reconstructed particles) and the ratio of the antiparallel component V_{AP} and the parallel component, V_P, of the hadronic final state. The two components are defined as

$$V_{AP} = -\sum_i \vec{p}_{T,i} \cdot \hat{n}, \quad \text{for } \vec{p}_{T,i} \cdot \hat{n} < 0, \tag{23}$$

and

$$V_P = \sum_i \vec{p}_{T,i} \cdot \hat{n}, \quad \text{for } \vec{p}_{T,i} \cdot \hat{n} > 0. \tag{24}$$

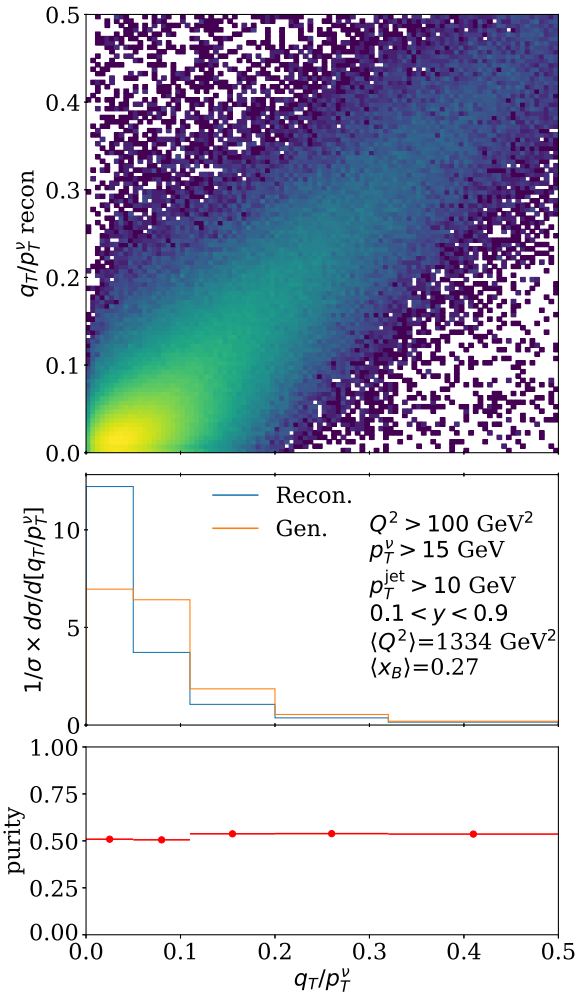

FIG. 8. Top: 2D histogram of the generated q_T/p_T^ν (x axis) vs the reconstructed value (y axis). Middle: spectra of reconstructed and generated q_T/p_T^ν. Bottom: purity as a function of q_T/p_T^ν.

Here $\vec{p}_{T,i}$ are the transverse parts of the individual particles' momenta, $\hat{n} = -\vec{p}_T^\nu/|\vec{p}_T^\nu|$, and we sum over all reconstructed particles in the event. The purpose of the cuts on this variable is to ensure an azimuthally collimated energy flow. For charged-current events, the ratio V_{AP}/V_P is small—in particular for the events that we are interested in for TMD studies.

In order to test the efficacy of these variables for background reduction, we ran simulations of photoproduction reactions in the same manner as our CC DIS simulations, see Sec. IV above. We focus on photoproduction because it is expected to be the dominant background, based on experience from HERA [33].

We used the following cuts: $p_T^\nu > 15$ GeV, $V_{AP}/V_P < 0.35$, and $\delta < 30$ GeV, which are similar to the values used in Ref. [33]. We found that ≈30% of the generated CC DIS events passed the cuts, whereas only $0.0005 \pm 0.0002\%$ of photoproduction events passed the cuts. However, the photoproduction cross section is three orders of magnitude

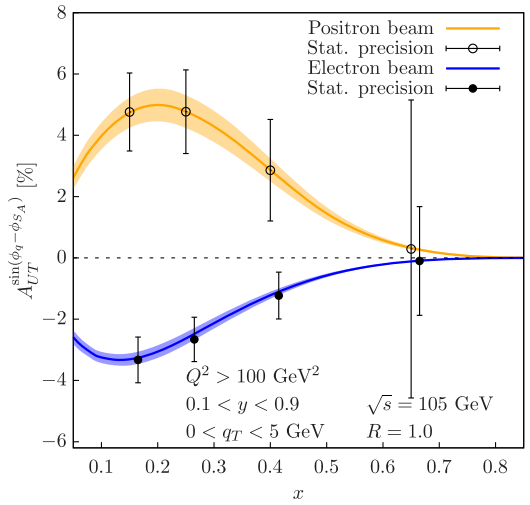

FIG. 9. Projected statistical precision for the neutrino-jet asymmetry, which is sensitive to the Sivers distribution, for e^+p collisions (open circles) and e^-p collision (closed circles), for 100 fb^{-1}. The yellow and blue curves show theoretical results and the corresponding bands show the uncertainty of the extracted Sivers function in Ref. [63].

larger compared to CC DIS (58 nb, compared to 14 pb, estimated using PYTHIA8). Therefore, we estimate that about $8 \pm 3\%$ of the identified event sample would be background from photoproduction when using only cuts on kinematic variables and no additional low-angle electron tagger.

Given that our estimate suggests that the background will be reduced to manageable levels, we neglect it from the projections we show in Sec. VII.

VII. STATISTICAL PRECISION OF SPIN ASYMMETRY MEASUREMENTS

In Fig. 9, we show the statistical uncertainty projected for the transverse single-spin asymmetry $A_{UT}^{\sin(\phi_q - \phi_{S_A})}$ as a function of Bjorken x. The bins in Bjorken x are sufficiently wide to reduce bin migration, given the resolution of the Jacquet-Blondel method (see Refs. [14,43]). Here we assume a luminosity of 100 fb^{-1} and the absolute uncertainty of the asymmetry measurement is estimated to be $\sqrt{2}/(p\sqrt{N})$, where p is the polarization of the proton beam, which we take to be 70%, and N is the number of events in a given bin that pass our cuts, scaled to match the next-to-leading-order total inclusive cross section of Ref. [43] and an integrated luminosity of 100 fb^{-1}. Following Ref. [115], we include a factor of $\sqrt{2}$ to account for the fitting of the azimuthal modulations.

We compare these results to the numerical results of our calculations, see Sec. III, which are integrated over the transverse-momentum imbalance $0 < q_T < 5$ GeV and inelasticity $0.1 < y < 0.9$. The uncertainty bands of the calculations show the uncertainty of current extractions of the Sivers function, see Ref. [63]. The projected statistical error bars are smaller than the predicted asymmetry for the first three bins, allowing the proposed measurement to provide a decent comparison to theoretical calculations.

While these measurements would provide weaker constraints on TMDs than analogous ones in the neutral-current channel, they offer an independent check with different flavor sensitivity. Moreover, they could test the consistency and universality of the theoretical predictions.

The measurement that is projected in Fig. 9 would require electron and positron beams. The capability to operate with positron beam is not included in the EIC baseline design although it might be a possible upgrade. Figure 9 shows that the positron data would yield an opposite asymmetry compared to the electron data, and their comparison could help constrain in particular the TMDs associated with the d quark. Within a global analysis, it will be possible to further demonstrate the impact and complementarity of the proposed jet observables to disentangle the flavor dependence of PDFs [56,58–65]. We leave dedicated studies for future work.

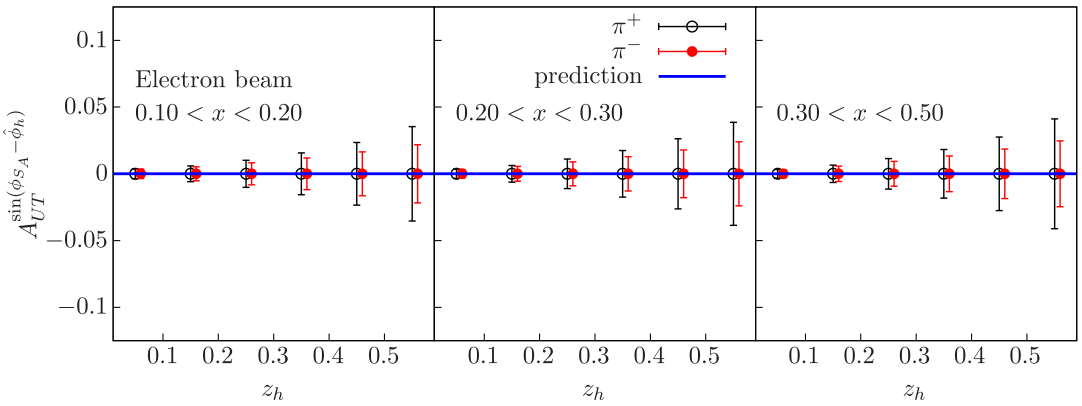

FIG. 10. Projected statistical precision for the z_h dependence of the $\pi^{\pm}$-in-jet Collins asymmetries (open circles for π^+, closed circles for π^-) in electron-proton collisions.

We likewise show in Fig. 10 the projected statistical uncertainties for hadron-in-jet Collins asymmetries as a function of z_h and Bjorken x for charged pions with $j_T < 1.5$ GeV. As explained in Sec. III, this asymmetry is expected to vanish in CC DIS within the TMD factorization formalism at leading power due to the chiral-odd nature of the transversity and Collins functions. The projected statistical uncertainties are at the level of 1% or smaller for small z_h. As we have mentioned earlier, performing these measurements will enable precise tests of the theory and the assumptions of factorization and chirality of the functions involved. If the asymmetry is not observed to be exactly zero, it might indicate sensitivity to subleading contributions that we have neglected in Sec. III or some other nonstandard effect.

VIII. SUMMARY AND CONCLUSIONS

We have proposed a novel channel to study the 3D structure of the nucleon at the EIC that offers unique sensitivity to different quark flavors: neutrino-jet correlations in charge-current deep-inelastic scattering.

We have presented first calculations of unpolarized cross-sections and transverse-spin asymmetries for this channel. In addition, we performed calculations of longitudinal and transverse momentum distributions of identified hadrons inside jets and we compared our results to Monte Carlo event-generator simulations. We find that the hadron-in-jet Collins asymmetry is exactly zero as a consequence of the chiral-odd nature of the effect.

We used the expected EIC machine parameters in terms of luminosity and energy to estimate the kinematic reach of the proposed measurement. We also used fast detector simulations to estimate the performance of the neutrino (missing-momentum) reconstruction, and the neutrino-jet momentum imbalance. We found that these measurements should be feasible with a general-purpose detector at the EIC running at nominal luminosity.

Jet-based TMD measurements in charged-current DIS will provide important cross-checks and complement analogous measurements in the neutral-current channel. As such, we conclude that this channel represents an interesting addition to the growing science program that can be carried out with jet measurements at the future EIC.

ACKNOWLEDGMENTS

This work was supported by the MRPI program of the University of California Office of the President, Award No. 00010100. M. A. was supported through DOE Contract No. DE-AC05-06OR23177 under which JSA operates the Thomas Jefferson National Accelerator Facility. Z. K. and F. Z. are supported by the National Science Foundation under Grant No. PHY-1945471. F. R. was supported by the Simons Foundation under the Simons Bridge program for Postdoctoral Fellowships at SCGP and YITP Award No. 815892; the NSF, Award No. 1915093; the DOE Contract No. DE-AC05-06OR23177, under which Jefferson Science Associates, LLC operates Jefferson Lab; and Old Dominion University. A. P. is supported by the National Science Foundation Grant No. PHY-2012002 and by the DOE Contract No. DE-AC05-06OR23177, under which Jefferson Science Associates, LLC operates Jefferson Lab.

APPENDIX A: INCLUSIVE JET PRODUCTION

In this appendix, we provide the expressions for all the structure functions that appear in Eq. (13). We start with the squared matrix element of the process $e + p \to \nu + \text{jet} + X$, where the incoming proton and electron are unpolarized, which is given by

$$\begin{aligned}
|\mathcal{M}|^2 &= \left(\frac{e^2}{2\sin^2\theta_w}\right)^2 |V_{ud}|^2 \frac{\left(g^{\mu\nu} - \frac{q^\mu q^\nu}{m_W^2}\right)\left(g^{\mu'\nu'} - \frac{q^{\mu'} q^{\nu'}}{m_W^2}\right)}{(q^2 - m_W^2)^2 + (m_W\Gamma_W)^2} \\
&\quad \times \mathrm{Tr}\left[\not{P}_D \gamma^\mu \left(\frac{1-\gamma_5}{2}\right) \not{P}_B \gamma^{\mu'} \left(\frac{1-\gamma_5}{2}\right)\right] \\
&\quad \times \mathrm{Tr}\left[\hat{\not{P}}_C \gamma^\nu \left(\frac{1-\gamma_5}{2}\right) \hat{\not{P}}_A \gamma^{\nu'} \left(\frac{1-\gamma_5}{2}\right)\right], \\
&= 8(G_F m_W^2)^2 |V_{ud}|^2 \frac{1}{(\hat{t} - m_W^2)^2 + (m_W\Gamma_W)^2} \\
&\quad \times \mathrm{Tr}\left[\not{P}_D \gamma^\mu \left(\frac{1-\gamma_5}{2}\right) \not{P}_B \gamma^\nu \left(\frac{1-\gamma_5}{2}\right)\right] \\
&\quad \times \mathrm{Tr}\left[\hat{\not{P}}_C \gamma_\mu \left(\frac{1-\gamma_5}{2}\right) \hat{\not{P}}_A \gamma_\nu \left(\frac{1-\gamma_5}{2}\right)\right]. \qquad \text{(A1)}
\end{aligned}$$

Here $\hat{P}_A = xP_A$ and $\hat{P}_C = P_J$ and we used $4G_F/\sqrt{2} = e^2/(2m_W^2\sin^2\theta_w)$. For a longitudinally polarized proton with helicity λ_p, we substitute $\hat{\not{P}}_A \to \gamma_5 \hat{\not{P}}_A$. For a transversely polarized proton with transverse spin S_T^i, we have $\hat{\not{P}}_A \to \gamma_5 \gamma_i \hat{\not{P}}_A$. However, note that the trace of the hadronic tensor vanishes for a transversely polarized proton. For a longitudinally polarized electron with helicity λ_e, one substitutes $\not{P}_B \to \not{P}_B + \lambda_e \gamma_5 \not{P}_B$. The leptonic tensor is given in terms of the momenta of the electron and the left-handed neutrino:

$$\begin{aligned}
L^{\mu\nu} &= \mathrm{Tr}\left[\not{P}_D \gamma^\mu (1 + \lambda_e\gamma_5) \not{P}_B \gamma^\nu \left(\frac{1-\gamma_5}{2}\right)\right], \\
&= (1 - \lambda_e)(P_B^\mu P_D^\nu + P_B^\nu P_D^\mu - g^{\mu\nu} P_B \cdot P_D + i\epsilon^{\mu\nu P_B P_D}), \\
&= L_u^{\mu\nu} + L_p^{\mu\nu}, \qquad \text{(A2)}
\end{aligned}$$

where

$$L_u^{\mu\nu} = (P_B^\mu P_D^\nu + P_B^\nu P_D^\mu - g^{\mu\nu} P_B \cdot P_D + i\epsilon^{\mu\nu P_B P_D}), \qquad \text{(A3)}$$

$$L_p^{\mu\nu} = -\lambda_e (P_B^\mu P_D^\nu + P_B^\nu P_D^\mu - g^{\mu\nu} P_B \cdot P_D + i\epsilon^{\mu\nu P_B P_D}), \qquad \text{(A4)}$$

represent the polarized and unpolarized components of the leptonic tensor. We can then obtain the differential cross section given in Eq. (13) with the following structure functions

$$\begin{aligned} F_{UU} &= \sum_q \frac{|\overline{\mathcal{M}}_{eq\to\nu q'}|^2}{16\pi^2\hat{s}^2} H(Q,\mu)\mathcal{J}_q(p_T^{\rm jet}R,\mu) \\ &\times \int \frac{{\rm d}b_T b_T}{2\pi} J_0(q_T b_T) f_1^{\rm TMD}(x,b_T,\mu,\zeta) \\ &\times S_q(b_T,y_{\rm jet},R,\mu), \\ &= \mathcal{C}[f_1]_{eq\to\nu q'}, \end{aligned} \tag{A5}$$

$$F_{LU} = \mathcal{C}[f_1]_{e_L q\to\nu q'}, \tag{A6}$$

$$F_{UL} = \mathcal{C}[g_{1L}]_{eq_L\to\nu q'}, \tag{A7}$$

$$F_{LL} = \mathcal{C}[g_{1L}]_{e_L q_L\to\nu q'}, \tag{A8}$$

$$\begin{aligned} F_{UT}^{\cos(\phi_q-\phi_{S_A})} &= \sum_q \frac{|\overline{\mathcal{M}}_{eq_L\to\nu q'}|^2}{16\pi^2\hat{s}^2} H(Q,\mu)\mathcal{J}_q(p_T^{\rm jet}R,\mu) \\ &\times \int \frac{{\rm d}b_T b_T^2}{4\pi M} J_1(q_T b_T) g_{1T}^{(1),\rm TMD}(x,b_T,\mu,\zeta) \\ &\times S_q(b_T,y_{\rm jet},R,\mu), \\ &= \tilde{\mathcal{C}}[g_{1T}]_{eq_L\to\nu q'}, \end{aligned} \tag{A9}$$

$$F_{LT}^{\cos(\phi_q-\phi_{S_A})} = \tilde{\mathcal{C}}[g_{1T}]_{e_L q_L\to\nu q'}, \tag{A10}$$

$$F_{UT}^{\sin(\phi_q-\phi_{S_A})} = \tilde{\mathcal{C}}[f_{1T}^{\perp}]_{eq\to\nu q'}, \tag{A11}$$

$$F_{LT}^{\sin(\phi_q-\phi_{S_A})} = \tilde{\mathcal{C}}[f_{1T}^{\perp}]_{e_L q\to\nu q'}. \tag{A12}$$

The relevant leading-order matrix elements squared are given by

$$|\overline{\mathcal{M}}_{eu\to\nu d}|^2 = 8(G_F m_W^2)^2 |V_{ud}|^2 \frac{\hat{s}^2}{(\hat{t}-m_W^2)^2+m_W^2\Gamma_W^2}, \tag{A13}$$

$$|\overline{\mathcal{M}}_{e\bar{d}\to\nu\bar{u}}|^2 = 8(G_F m_W^2)^2 |V_{ud}|^2 \frac{\hat{u}^2}{(\hat{t}-m_W^2)^2+m_W^2\Gamma_W^2}, \tag{A14}$$

$$|\overline{\mathcal{M}}_{e_L q\to\nu q'}|^2 = -|\overline{\mathcal{M}}_{eq\to\nu q'}|^2, \tag{A15}$$

$$|\overline{\mathcal{M}}_{eq_L\to\nu q'}|^2 = -|\overline{\mathcal{M}}_{eq\to\nu q'}|^2, \tag{A16}$$

$$|\overline{\mathcal{M}}_{e_L q_L\to\nu q'}|^2 = |\overline{\mathcal{M}}_{eq\to\nu q'}|^2, \tag{A17}$$

The matrix elements for an unpolarized and polarized electron are related to each other, see Eqs. (A16), (A17) due to the factor $(1-\lambda_e)$ in the expression of the leptonic tensor. As a result, we obtain the following relations between the different structure functions:

$$F_{LU} = -F_{UU}, \tag{A18}$$

$$F_{LL} = -F_{UL}, \tag{A19}$$

$$F_{LT}^{\cos(\phi_q-\phi_{S_A})} = -F_{UT}^{\cos(\phi_q-\phi_{S_A})}, \tag{A20}$$

$$F_{LT}^{\sin(\phi_q-\phi_{S_A})} = -F_{UT}^{\sin(\phi_q-\phi_{S_A})}. \tag{A21}$$

APPENDIX B: HADRON DISTRIBUTIONS INSIDE THE JET

For an unpolarized final-state hadron, we obtain TMD jet fragmentation functions $\mathcal{D}_1$, $\mathcal{H}_1^{\perp}$ at leading twist [20]. The corresponding correlator can be written as follows:

$$\Delta(z_h,\vec{j}_T) = \mathcal{D}_1^{h/q}(z_h,j_T)\frac{\not{n}_-}{2} - i\mathcal{H}_1^{\perp,h/q}(z_h,j_T)\frac{\not{j}_T}{z_h M_h}\frac{\not{n}_-}{2}, \tag{B1}$$

where we suppress the dependence on the renormalization scale μ and the Collins-Soper scale ζ [78]. The different traces of the correlator are given by

$$\Delta^{h/q[\gamma^-]} = \mathcal{D}_1^{h/q}(z_h,j_T), \tag{B2}$$

$$\Delta^{h/q[i\sigma^{i-}\gamma_5]} = \frac{\epsilon_T^{ij}j_T^{\,j}}{z_h M_h}\mathcal{H}_1^{\perp,h/q}(z_h,j_T). \tag{B3}$$

For an electron colliding with an unpolarized or a longitudinally polarized initial proton, we obtain the same partonic scattering amplitudes as shown in Appendix A. However, if the electron collides with a transversely polarized quark from the initial proton, the corresponding term in the hadronic tensor is given by

$$H^{\mu\nu}_{\mathcal{H}_1^{\perp h/q}} = {\rm Tr}\left[\frac{\not{j}_T}{z_h M_h}\hat{\not{P}}_C\gamma^\mu\left(\frac{1-\gamma_5}{2}\right)\not{n}_+\hat{\not{P}}_A\gamma^\nu\left(\frac{1-\gamma_5}{2}\right)\right], \tag{B4}$$

where $\hat{P}_A = xP_A$ and $\hat{P}_C = P_J$. For different TMD PDFs, the vector $\not{v}$ is given by $(-\not{S}_T\gamma_5)$ for h_1, $(-\lambda_p\not{k}_T\gamma_5/M)$ for $h_{1L}^{\perp}$, $(-i\not{k}_T/M)$ for $h_1^{\perp}$ and $((\vec{k}_T\cdot\vec{S}_T\not{k}_T-\vec{k}_T^2\not{S}_T/2)\gamma_5/M^2)$ for $h_{1T}^{\perp}$. Note that there are always three γ matrices between the $(1-\gamma_5)/2$ factors in the expression of the hadronic tensor in Eq. (B4). Thus, we find

$$\left(\frac{1-\gamma_5}{2}\right)\gamma_\alpha\gamma_\beta\gamma_\rho\left(\frac{1-\gamma_5}{2}\right) = \gamma_\alpha\gamma_\beta\gamma_\rho\left(\frac{1+\gamma_5}{2}\right)\left(\frac{1-\gamma_5}{2}\right) = 0. \tag{B5}$$

Therefore, the expression in Eq. (B4) vanishes and spin asymmetries involving transversely polarized quarks in CC DIS are zero. As a result, all contributions related to chiral-odd Collins jet fragmentation function do not appear in the differential cross section for hadron-in-jet production. Here, we show the differential cross section in terms of the remaining nonzero structure functions

$$\begin{aligned}\frac{\mathrm{d}\sigma^{ep\to\nu+\mathrm{jet}X}}{\mathrm{d}y_J\mathrm{d}^2p_{JT}\mathrm{d}^2q_T\mathrm{d}z_h\mathrm{d}^2j_T} &= F^h_{UU} + \lambda_p F^h_{UL} + |S_T|\Big[\cos(\phi_q-\phi_{S_A})F^{h,\cos(\phi_q-\phi_{S_A})}_{UT} \\ &+ \sin(\phi_q-\phi_{S_A})F^{h,\sin(\phi_q-\phi_{S_A})}_{UT}\Big] \\ &+ \lambda_e\Big[F^h_{LU} + |S_T|\sin(\phi_q-\phi_{S_A})F^{h,\sin(\phi_q-\phi_{S_A})}_{LT} \\ &+ \lambda_p F^h_{LL} + |S_T|\cos(\phi_q-\phi_{S_A})F^{h,\cos(\phi_q-\phi_{S_A})}_{LT}\Big)\Big].\end{aligned} \tag{B6}$$

In total there are eight structure functions, which are given by

$$\begin{aligned}F^h_{UU} &= \sum_q \frac{|\overline{\mathcal{M}}_{eq\to\nu q'}|^2}{16\pi^2\hat{s}^2}H(Q,\mu)\mathcal{D}_1(p_T^{\mathrm{jet}}R,\mu) \\ &\times\int\frac{\mathrm{d}b_T b_T}{2\pi}J_0(q_T b_T)f_1^{\mathrm{TMD}}(x,b_T,\mu,\zeta) \\ &\times S_q(b_T,y_{\mathrm{jet}},R,\mu), \\ &= \mathcal{C}^h[f_1\mathcal{D}_1]_{eq\to\nu q'},\end{aligned} \tag{B7}$$

$$F^h_{LU} = \mathcal{C}^h[f_1\mathcal{D}_1]_{e_Lq\to\nu q'}, \tag{B8}$$

$$F^h_{UL} = \mathcal{C}^h[g_{1L}\mathcal{D}_1]_{eq_L\to\nu q'}, \tag{B9}$$

$$F^h_{LL} = \mathcal{C}^h[g_{1L}\mathcal{D}_1]_{e_Lq_L\to\nu q'}, \tag{B10}$$

$$\begin{aligned}F^{h,\cos(\phi_q-\phi_{S_A})}_{UT} &= \sum_q \frac{|\overline{\mathcal{M}}_{eq_L\to\nu q'}|^2}{16\pi^2\hat{s}^2}H(Q,\mu)\mathcal{D}_1(p_T^{\mathrm{jet}}R,\mu) \\ &\times\int\frac{\mathrm{d}b_T b_T^2}{4\pi M}J_1(q_T b_T)g_{1T}^{(1),\mathrm{TMD}}(x,b_T,\mu,\zeta) \\ &\times S_q(b_T,y_{\mathrm{jet}},R,\mu), \\ &= \tilde{\mathcal{C}}^h[g_{1T}\mathcal{D}_1/M]_{eq_L\to\nu q'},\end{aligned} \tag{B11}$$

$$F^{h,\cos(\phi_q-\phi_{S_A})}_{LT} = \tilde{\mathcal{C}}^h[g_{1T}\mathcal{D}_1/M]_{e_Lq_L\to\nu q'}, \tag{B12}$$

$$F^{h,\sin(\phi_q-\phi_{S_A})}_{UT} = \tilde{\mathcal{C}}^h[f_{1T}^\perp\mathcal{D}_1/M]_{eq\to\nu q'}, \tag{B13}$$

$$F^{h,\sin(\phi_q-\phi_{S_A})}_{LT} = \tilde{\mathcal{C}}^h[f_{1T}^\perp\mathcal{D}_1/M]_{e_Lq\to\nu q'}. \tag{B14}$$

We can obtain relations between the different hadron-in-jet structure functions analogous to inclusive jets production (see Appendix A):

$$F^h_{LU} = -F^h_{UU}, \tag{B15}$$

$$F^h_{LL} = -F^h_{UL}, \tag{B16}$$

$$F^{h,\cos(\phi_q-\phi_{S_A})}_{LT} = -F^{h,\cos(\phi_q-\phi_{S_A})}_{UT}, \tag{B17}$$

$$F^{h,\sin(\phi_q-\phi_{S_A})}_{LT} = -F^{h,\sin(\phi_q-\phi_{S_A})}_{UT}. \tag{B18}$$

[1] A. Accardi *et al.*, Electron ion collider: The next QCD frontier, Eur. Phys. J. A **52**, 268 (2016).

[2] R. Abdul Khalek *et al.*, Science requirements and detector concepts for the electron-ion collider: EIC yellow report, Nucl. Phys. **A1026**, 122447 (2022).

[3] M. Arratia, Y. Song, F. Ringer, and B. Jacak, Jets as precision probes in electron-nucleus collisions at the electron-ion collider, Phys. Rev. C **101**, 065204 (2020).

[4] B. S. Page, X. Chu, and E. C. Aschenauer, Experimental aspects of jet physics at a future EIC, Phys. Rev. D **101**, 072003 (2020).

[5] Z.-B. Kang, A. Metz, J.-W. Qiu, and J. Zhou, Exploring the structure of the proton through polarization observables in $lp \to \mathrm{jet}X$, Phys. Rev. D **84**, 034046 (2011).

[6] P. Hinderer, M. Schlegel, and W. Vogelsang, Single-inclusive production of hadrons and jets in lepton-nucleon scattering at NLO, Phys. Rev. D **92**, 014001 (2015).

[7] R. Boughezal, F. Petriello, and H. Xing, Inclusive jet production as a probe of polarized parton distribution functions at a future EIC, Phys. Rev. D **98**, 054031 (2018).

[8] L. Zheng, E. C. Aschenauer, J. H. Lee, B.-W. Xiao, and Z.-B. Yin, Accessing the gluon Sivers function at a future electron-ion collider, Phys. Rev. D **98**, 034011 (2018).

[9] D. Gutierrez-Reyes, I. Scimemi, W. J. Waalewijn, and L. Zoppi, Transverse Momentum Dependent Distributions with Jets, Phys. Rev. Lett. **121**, 162001 (2018).

[10] D. Gutierrez-Reyes, I. Scimemi, W. J. Waalewijn, and L. Zoppi, Transverse momentum dependent distributions in

e^+e^- and semi-inclusive deep-inelastic scattering using jets, J. High Energy Phys. 10 (2019) 031.
[11] X. Liu, F. Ringer, W. Vogelsang, and F. Yuan, Lepton-jet Correlations in Deep Inelastic Scattering at the Electron-Ion Collider, Phys. Rev. Lett. **122**, 192003 (2019).
[12] Z.-B. Kang, K. Lee, and F. Zhao, Polarized jet fragmentation functions, Phys. Lett. B **809**, 135756 (2020).
[13] I. Borsa, D. de Florian, and I. Pedron, Inclusive-jet and dijet production in polarized deep inelastic scattering, Phys. Rev. D **103**, 014008 (2021).
[14] M. Arratia, Y. Furletova, T. J. Hobbs, F. Olness, and S. J. Sekula, Charm jets as a probe for strangeness at the future electron-ion collider, Phys. Rev. D **103**, 074023 (2021).
[15] M. Arratia, Z.-B. Kang, A. Prokudin, and F. Ringer, Jet-based measurements of Sivers and Collins asymmetries at the future electron-ion collider, Phys. Rev. D **102**, 074015 (2020).
[16] X. Liu, F. Ringer, W. Vogelsang, and F. Yuan, Lepton-jet correlation in deep inelastic scattering, Phys. Rev. D **102**, 094022 (2020).
[17] M. Arratia, Y. Makris, D. Neill, F. Ringer, and N. Sato, Asymmetric jet clustering in deep-inelastic scattering, Phys. Rev. D **104**, 034005 (2021).
[18] Z.-B. Kang, X. Liu, S. Mantry, and D. Y. Shao, Jet Charge: A Flavor Prism for Spin Asymmetries at the EIC, Phys. Rev. Lett. **125**, 242003 (2020).
[19] V. Guzey and M. Klasen, Diffractive dijet photoproduction at the EIC, J. High Energy Phys. 05 (2020) 074.
[20] Z.-B. Kang, K. Lee, D. Y. Shao, and F. Zhao, Spin asymmetries in electron-jet production at the future electron ion collider, J. High Energy Phys. 11 (2021) 005.
[21] R. F. del Castillo, M. G. Echevarria, Y. Makris, and I. Scimemi, Transverse momentum dependent distributions in dijet and heavy hadron pair production at EIC, J. High Energy Phys. 03 (2022) 047.
[22] Y. Makris, Revisiting the role of grooming in DIS, Phys. Rev. D **103**, 054005 (2021).
[23] Y.-Y. Zhang and X.-N. Wang, Parton rescattering and gluon saturation in dijet production at EIC, Phys. Rev. D **105**, 034015 (2022).
[24] H. T. Li, B. Yan, and C. P. Yuan, Jet charge: A new tool to probe the anomalous $Zb\bar{b}$ couplings at the EIC, Phys. Lett. B **833**, 137300 (2022).
[25] B. Yan, Z. Yu, and C. P. Yuan, The anomalous $Zb\bar{b}$ couplings at the HERA and EIC, Phys. Lett. B **822**, 136697 (2021).
[26] R. Abdul Khalek *et al.*, Snowmass 2021 white paper: Electron ion collider for high energy physics, in *2022 Snowmass Summer Study*, arXiv:2203.13199.
[27] X.-B. Tong, B.-W. Xiao, and Y.-Y. Zhang, Harmonics of Parton Saturation in Lepton-Jet Correlations at the EIC, Phys. Rev. Lett. **130**, 151902 (2023).
[28] X. Liu and H. X. Zhu, The Nucleon Energy Correlators, Phys. Rev. Lett. **130**, 091901 (2023).
[29] K. Lee, J. Mulligan, M. Płoskoń, F. Ringer, and F. Yuan, Machine learning-based jet and event classification at the electron-ion collider with applications to hadron structure and spin physics, J. High Energy Phys. 03 (2023) 085.
[30] J. Arrington *et al.*, EIC physics from an all-silicon tracking detector, arXiv:2102.08337.
[31] B. Pire, L. Szymanowski, and J. Wagner, Charged current electroproduction of a charmed meson at an electron-ion collider, Phys. Rev. D **104**, 094002 (2021).
[32] F. Aaron *et al.* (H1 Collaboration), Inclusive deep inelastic scattering at high Q^2 with longitudinally polarised lepton beams at HERA, J. High Energy Phys. 09 (2012) 061.
[33] H. Abramowicz *et al.* (ZEUS Collaboration), Measurement of high-Q^2 charged current deep inelastic scattering cross sections with a longitudinally polarised positron beam at HERA, Eur. Phys. J. C **70**, 945 (2010).
[34] S. Chekanov *et al.* (ZEUS Collaboration), Measurement of charged current deep inelastic scattering cross sections with a longitudinally polarised electron beam at HERA, Eur. Phys. J. C **61**, 223 (2009).
[35] S. Chekanov *et al.* (ZEUS Collaboration), Measurement of high Q^2 charged current cross-sections in e^-p deep inelastic scattering at HERA, Phys. Lett. B **539**, 197 (2002); **552**, 308(E) (2003).
[36] J. Breitweg *et al.* (ZEUS Collaboration), Measurement of high Q**2 charged current e + p deep inelastic scattering cross-sections at HERA, Eur. Phys. J. C **12**, 411 (2000).
[37] M. Derrick *et al.* (ZEUS Collaboration), Study of charged current ep interactions at $Q^2 > 200\text{-Gev}^2$ with the ZEUS detector at HERA, Z. Phys. C **72**, 47 (1996).
[38] H. Abramowicz *et al.* (H1, ZEUS Collaboration), Combination of measurements of inclusive deep inelastic $e^{\pm}p$ scattering cross sections and QCD analysis of HERA data, Eur. Phys. J. C **75**, 580 (2015).
[39] S. Chekanov *et al.* (ZEUS Collaboration), Jet production in charged current deep inelastic e + p scattering at HERA, Eur. Phys. J. C **31**, 149 (2003).
[40] S. Chekanov *et al.* (ZEUS Collaboration), Multi-jet cross-sections in charged current e + -p scattering at HERA, Phys. Rev. D **78**, 032004 (2008).
[41] T. Gehrmann, A. Huss, J. Niehues, A. Vogt, and D. M. Walker, Jet production in charged-current deep-inelastic scattering to third order in QCD, Phys. Lett. B **792**, 182 (2019).
[42] J. Blumlein, The theory of deeply inelastic scattering, Prog. Part. Nucl. Phys. **69**, 28 (2013).
[43] E. C. Aschenauer, T. Burton, T. Martini, H. Spiesberger, and M. Stratmann, Prospects for charged current deep-inelastic scattering off polarized nucleons at a future electron-ion collider, Phys. Rev. D **88**, 114025 (2013).
[44] H. Avakian, B. Parsamyan, and A. Prokudin, Spin orbit correlations and the structure of the nucleon, Riv. Nuovo Cimento **42**, 1 (2019).
[45] M. Anselmino, P. Gambino, and J. Kalinowski, Polarized deep inelastic scattering at high-energies and parity violating structure functions, Z. Phys. C **64**, 267 (1994).
[46] K.-b. Chen and W.-h. Yang, Parity violating semi-inclusive deeply inelastic scattering at the electron-ion collider, Phys. Rev. D **101**, 096017 (2020).
[47] W.-h. Yang, Charged current semi-inclusive deeply inelastic scattering at the electron-ion collider, Phys. Rev. D **103**, 016011 (2021).
[48] X. Yang and W. Yang, Semi-inclusive deeply inelastic (anti)neutrino nucleus scattering, arXiv:2211.10899.

[49] A. Gao, J. K. L. Michel, I. W. Stewart, and Z. Sun, A better angle on hadron transverse momentum distributions at the EIC, arXiv:2209.11211.

[50] F. Yuan, Azimuthal Asymmetric Distribution of Hadrons Inside a Jet at Hadron Collider, Phys. Rev. Lett. **100**, 032003 (2008).

[51] M. Procura and I. W. Stewart, Quark fragmentation within an identified jet, Phys. Rev. D **81**, 074009 (2010); **83**, 039902(E) (2011).

[52] Z.-B. Kang, X. Liu, F. Ringer, and H. Xing, The transverse momentum distribution of hadrons within jets, J. High Energy Phys. 11 (2017) 068.

[53] P. Sun, J. Isaacson, C. P. Yuan, and F. Yuan, Nonperturbative functions for SIDIS and Drell–Yan processes, Int. J. Mod. Phys. A **33**, 1841006 (2018).

[54] A. Bacchetta, F. Delcarro, C. Pisano, M. Radici, and A. Signori, Extraction of partonic transverse momentum distributions from semi-inclusive deep-inelastic scattering, Drell-Yan and Z-boson production, J. High Energy Phys. 06 (2017) 081.

[55] I. Scimemi and A. Vladimirov, Non-perturbative structure of semi-inclusive deep-inelastic and Drell-Yan scattering at small transverse momentum, J. High Energy Phys. 06 (2020) 137.

[56] J. Cammarota, L. Gamberg, Z.-B. Kang, J. A. Miller, D. Pitonyak, A. Prokudin, T. C. Rogers, and N. Sato (Jefferson Lab Angular Momentum Collaboration), Origin of single transverse-spin asymmetries in high-energy collisions, Phys. Rev. D **102**, 054002 (2020).

[57] A. Bacchetta, V. Bertone, C. Bissolotti, G. Bozzi, M. Cerutti, F. Piacenza, M. Radici, and A. Signori (MAP Collaboration), Unpolarized transverse momentum distributions from a global fit of Drell-Yan and semi-inclusive deep-inelastic scattering data, J. High Energy Phys. 10 (2022) 127.

[58] P. Sun and F. Yuan, Energy evolution for the sivers asymmetries in hard processes, Phys. Rev. D **88**, 034016 (2013).

[59] M. G. Echevarria, A. Idilbi, Z.-B. Kang, and I. Vitev, QCD evolution of the sivers asymmetry, Phys. Rev. D **89**, 074013 (2014).

[60] M. Anselmino, M. Boglione, U. D'Alesio, F. Murgia, and A. Prokudin, Study of the sign change of the Sivers function from STAR Collaboration W/Z production data, J. High Energy Phys. 04 (2017) 046.

[61] M. Boglione, U. D'Alesio, C. Flore, and J. O. Gonzalez-Hernandez, Assessing signals of TMD physics in SIDIS azimuthal asymmetries and in the extraction of the Sivers function, J. High Energy Phys. 07 (2018) 148.

[62] A. Bacchetta, F. Delcarro, C. Pisano, and M. Radici, The 3-dimensional distribution of quarks in momentum space, Phys. Lett. B **827**, 136961 (2022).

[63] M. G. Echevarria, Z.-B. Kang, and J. Terry, Global analysis of the Sivers functions at NLO + NNLL in QCD, J. High Energy Phys. 01 (2021) 126.

[64] M. Bury, A. Prokudin, and A. Vladimirov, Extraction of the Sivers Function from SIDIS, Drell-Yan, and $W^{\pm}/Z$ Data at Next-to-Next-to-Next-to Leading Order, Phys. Rev. Lett. **126**, 112002 (2021).

[65] M. Bury, A. Prokudin, and A. Vladimirov, Extraction of the Sivers function from SIDIS, Drell-Yan, and $W^{\pm}/Z$ boson production data with TMD evolution, J. High Energy Phys. 05 (2021) 151.

[66] I. P. Fernando and D. Keller, A modern global extraction of the sivers function, arXiv:2304.14328.

[67] M. Anselmino, M. Boglione, U. D'Alesio, S. Melis, F. Murgia, and A. Prokudin, Simultaneous extraction of transversity and Collins functions from new SIDIS and e + e− data, Phys. Rev. D **87**, 094019 (2013).

[68] Z.-B. Kang, A. Prokudin, P. Sun, and F. Yuan, Extraction of quark transversity distribution and collins fragmentation functions with QCD evolution, Phys. Rev. D **93**, 014009 (2016).

[69] M. Radici, A. Courtoy, A. Bacchetta, and M. Guagnelli, Improved extraction of valence transversity distributions from inclusive dihadron production, J. High Energy Phys. 05 (2015) 123.

[70] M. Radici and A. Bacchetta, First Extraction of Transversity from a Global Analysis of Electron-Proton and Proton-Proton Data, Phys. Rev. Lett. **120**, 192001 (2018).

[71] J. Benel, A. Courtoy, and R. Ferro-Hernandez, A constrained fit of the valence transversity distributions from dihadron production, Eur. Phys. J. C **80**, 465 (2020).

[72] U. D'Alesio, C. Flore, and A. Prokudin, Role of the Soffer bound in determination of transversity and the tensor charge, Phys. Lett. B **803**, 135347 (2020).

[73] L. Gamberg, M. Malda, J. A. Miller, D. Pitonyak, A. Prokudin, and N. Sato (Jefferson Lab Angular Momentum (JAM) Collaboration), Updated QCD global analysis of single transverse-spin asymmetries: Extracting $\tilde{H}$, and the role of the Soffer bound and lattice QCD, Phys. Rev. D **106**, 034014 (2022).

[74] Z.-B. Kang, K. Lee, D. Y. Shao, and F. Zhao, Spin asymmetries in electron-jet production at the EIC, J. Phys. Soc. Jpn. Conf. Proc. **37**, 020128 (2022).

[75] S. D. Ellis, C. K. Vermilion, J. R. Walsh, A. Hornig, and C. Lee, Jet shapes and jet algorithms in SCET, J. High Energy Phys. 11 (2010) 101.

[76] M. Cacciari, G. P. Salam, and G. Soyez, The anti-k_t jet clustering algorithm, J. High Energy Phys. 04 (2008) 063.

[77] D. Boer, L. Gamberg, B. Musch, and A. Prokudin, Bessel-weighted asymmetries in semi inclusive deep inelastic scattering, J. High Energy Phys. 10 (2011) 021.

[78] J. Collins, *Foundations of Perturbative QCD* (Cambridge University Press, Cambridge, England, 2013), Vol. 32.

[79] J. C. Collins, D. E. Soper, and G. F. Sterman, Transverse momentum distribution in Drell-Yan pair and W and Z boson production, Nucl. Phys. **B250**, 199 (1985).

[80] S. M. Aybat and T. C. Rogers, TMD parton distribution and fragmentation functions with QCD evolution, Phys. Rev. D **83**, 114042 (2011).

[81] M.-x. Luo, T.-Z. Yang, H. X. Zhu, and Y. J. Zhu, Quark Transverse Parton Distribution at the Next-to-Next-to-Next-to-Leading Order, Phys. Rev. Lett. **124**, 092001 (2020).

[82] M.-x. Luo, T.-Z. Yang, H. X. Zhu, and Y. J. Zhu, Unpolarized quark and gluon TMD PDFs and FFs at N^3LO, J. High Energy Phys. 06 (2021) 115.

[83] M. A. Ebert, B. Mistlberger, and G. Vita, Transverse momentum dependent PDFs at N^3LO, J. High Energy Phys. 09 (2020) 146.
[84] M. A. Ebert, A. Gao, and I. W. Stewart, Factorization for azimuthal asymmetries in SIDIS at next-to-leading power, J. High Energy Phys. 06 (2022) 007.
[85] S. Rodini and A. Vladimirov, Definition and evolution of transverse momentum dependent distribution of twist-three, J. High Energy Phys. 08 (2022) 031.
[86] L. Gamberg, Z.-B. Kang, D. Y. Shao, J. Terry, and F. Zhao, Transverse-momentum-dependent factorization at next-to-leading power, arXiv:2211.13209.
[87] S. Benic, Y. Hatta, H.-n. Li, and D.-J. Yang, Single-spin asymmetries at two loops, Phys. Rev. D **100**, 094027 (2019).
[88] S. Benić, Y. Hatta, A. Kaushik, and H.-n. Li, gT(x) contribution to single spin asymmetries in SIDIS, Phys. Rev. D **104**, 094027 (2021).
[89] A. Jain, M. Procura, and W. J. Waalewijn, Parton fragmentation within an identified jet at NNLL, J. High Energy Phys. 05 (2011) 035.
[90] T. Kaufmann, A. Mukherjee, and W. Vogelsang, Hadron fragmentation inside jets in hadronic collisions, Phys. Rev. D **92**, 054015 (2015).
[91] Z.-B. Kang, F. Ringer, and I. Vitev, Jet substructure using semi-inclusive jet functions in SCET, J. High Energy Phys. 11 (2016) 155.
[92] R. Bain, Y. Makris, and T. Mehen, Transverse momentum dependent fragmenting jet functions with applications to quarkonium production, J. High Energy Phys. 11 (2016) 144.
[93] Z.-B. Kang, A. Prokudin, F. Ringer, and F. Yuan, Collins azimuthal asymmetries of hadron production inside jets, Phys. Lett. B **774**, 635 (2017).
[94] Z.-B. Kang, K. Lee, J. Terry, and H. Xing, Jet fragmentation functions for *Z*-tagged jets, Phys. Lett. B **798**, 134978 (2019).
[95] D. de Florian, R. Sassot, M. Epele, R. J. Hernández-Pinto, and M. Stratmann, Parton-to-pion fragmentation reloaded, Phys. Rev. D **91**, 014035 (2015).
[96] T. Sjostrand, S. Mrenna, and P. Z. Skands, A brief introduction to PYTHIA8.1, Comput. Phys. Commun. **178**, 852 (2008).
[97] BNL, An electron-ion collider study, https://wiki.bnl.gov/eic/upload/EIC.Design.Study.pdf (2020).
[98] B. Badelek, D. Y. Bardin, K. Kurek, and C. Scholz, Radiative correction schemes in deep inelastic muon scattering, Z. Phys. C **66**, 591 (1995).
[99] T. Liu, W. Melnitchouk, J.-W. Qiu, and N. Sato, A new approach to semi-inclusive deep-inelastic scattering with QED and QCD factorization, J. High Energy Phys. 11 (2021) 157.
[100] V. Andreev *et al.* (H1 Collaboration), Measurement of Lepton-Jet Correlation in Deep-Inelastic Scattering with the H1 Detector Using Machine Learning for Unfolding, Phys. Rev. Lett. **128**, 132002 (2022).
[101] M. Cacciari, G. P. Salam, and G. Soyez, FastJet user manual, Eur. Phys. J. C **72**, 1896 (2012).
[102] J. de Favereau, C. Delaere, P. Demin, A. Giammanco, V. Lemaître, A. Mertens, and M. Selvaggi (DELPHES3 Collaboration), DELPHES3, A modular framework for fast simulation of a generic collider experiment, J. High Energy Phys. 02 (2014) 057.
[103] M. Arratia and S. Sekula, A Delphes card for the EIC yellow-report detector, arXiv:2103.06886.
[104] J. K. Adkins *et al.*, Design of the ECCE detector for the electron ion collider, arXiv:2209.02580.
[105] J. Adam *et al.* (ATHENA Collaboration), ATHENA detector proposal—a totally hermetic electron nucleus apparatus proposed for IP6 at the Electron-Ion Collider, J. Instrum. **17**, P10019 (2022).
[106] R. Alarcon *et al.* (CORE Collaboration), CORE—a compact detector for the EIC, arXiv:2209.00496.
[107] M. Arratia *et al.*, A high-granularity calorimeter insert based on SiPM-on-tile technology at the future electron-ion collider, Nucl. Instrum. Methods Phys. Res., Sect. A **1047**, 167866 (2023).
[108] P. Newman and M. Wing, The hadronic final state at HERA, Rev. Mod. Phys. **86**, 1037 (2014).
[109] B. I. Abelev *et al.* (STAR Collaboration), Measurement of Transverse Single-Spin Asymmetries for Di-Jet Production in Proton-Proton Collisions at $s^{**}(1/2) = 200$-GeV, Phys. Rev. Lett. **99**, 142003 (2007).
[110] U. Amaldi *et al.*, Report from the study group on detectors for charged current events, in *ECFA Study of an ep Facility for Europe* (1979).
[111] M. Arratia, D. Britzger, O. Long, and B. Nachman, Reconstructing the kinematics of deep inelastic scattering with deep learning, Nucl. Instrum. Methods Phys. Res., Sect. A **1025**, 166164 (2022).
[112] M. Diefenthaler, A. Farhat, A. Verbytskyi, and Y. Xu, Deeply learning deep inelastic scattering kinematics, Eur. Phys. J. C **82**, 1064 (2022).
[113] M. Arratia, D. Britzger, O. Long, and B. Nachman, Optimizing observables with machine learning for better unfolding, J. Instrum. **17**, P07009 (2022).
[114] C. Pecar and A. Vossen, Reconstruction of event kinematics in semi-inclusive deep-inelastic scattering using the hadronic final state and Machine Learning, arXiv:2209.14489.
[115] M. Anselmino *et al.*, Transverse momentum dependent parton distribution/fragmentation functions at an electron-ion collider, Eur. Phys. J. A **47**, 35 (2011).